Journal of Polymers and the Environment (2022) 30:4463–4478
https://doi.org/10.1007/s10924-022-02530-1

ORIGINAL PAPER

Adsorptive Removal of Lead from Water Using a Novel Cysteine-Bentonite/Poly(vinyl alcohol)/Alginate Nanocomposite

Tahereh Salehi[1] · Mehran Shirvani[1] · Mohammad Dinari[2] · Edris Gavili[1]

Accepted: 4 July 2022 / Published online: 19 July 2022

Abstract

Adsorptive removal of toxic metals from water using materials with high removal capability and sufficient environmental degradability is of great importance. In this study, a novel nanocomposite adsorbent was synthesized by reinforcing poly(vinyl alcohol)/alginate (PVA/Alg) hydrogel using cysteine-modified bentonite (Cys-BNT). The synthesized composite was characterized using XRD, FTIR, and TEM techniques and subsequently used to remove Pb from aqueous solutions. The factors that affect the Pb adsorption of the composite, including solution pH, Pb concentration, and time were also evaluated. The XRD and TEM results revealed the coexistence of exfoliated and intercalated BNT layers in the polymer matrix. The Pb removal was pH-dependent with the highest Pb removal efficiency at pH 5.0. The incorporation of Cys-BNT significantly ($P < 0.05$) enhanced the maximum Pb adsorption capacity of PVA/Alg hydrogel from 480 to 995 μmol g^{-1}. The Elovich model was the best to fit the Pb adsorption kinetic data, and the adsorption equilibrium time was 4 h. The Pb removal rate was also significantly ($P < 0.05$) increased through embedding the Cys-BNT into the PVA/Alg hybrid. Overall, the prepared Cys-BNT/PVA/Alg nanocomposite exhibits a great adsorption efficiency and a rapid adsorption behavior, making it a suitable material to remove Pb from polluted waters.

✉ Mehran Shirvani
shirvani@iut.ac.ir

[1] Department of Soil Science, College of Agriculture, Isfahan University of Technology, Isfahan 84156-83111, Iran

[2] Department of Chemistry, Isfahan University of Technology, Isfahan 84156-83111, Iran

Graphical Abstract

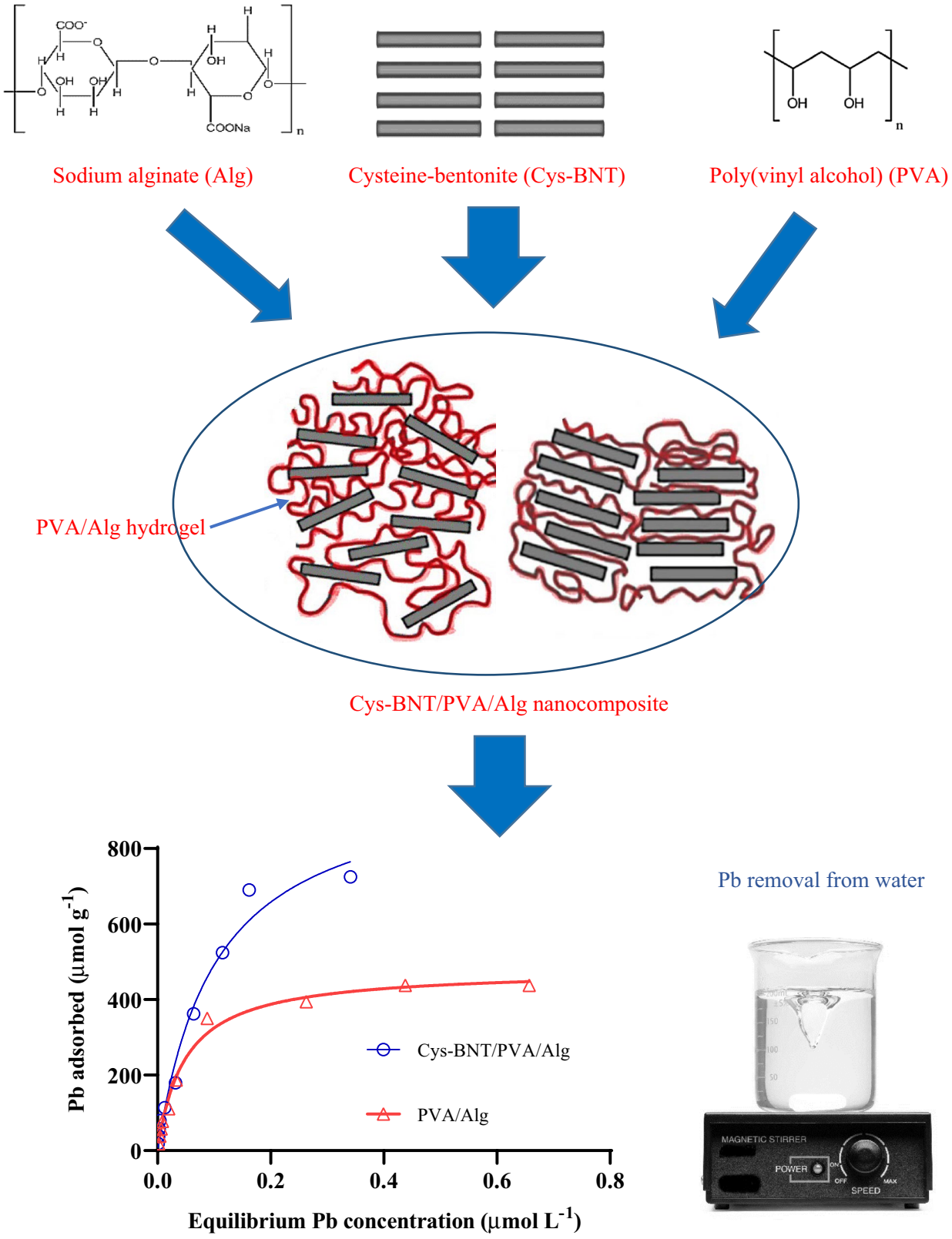

Keywords Montmorillonite · Clay minerals · Cysteine · Pb · Hybrid materials · Water purification

Introduction

Water pollution is a worldwide crisis caused by various chemicals released from agricultural, industrial, and municipal activities, leading to enormous economic, environmental, and human health problems [1]. Lead (Pb) is among the most hazardous metals commonly found in polluted waters, affecting human health worldwide by inducing detrimental health disorders such as damage to the nervous, renal, and reproductive systems [2, 3]. According to the US Environmental Protection Agency (EPA), the maximum permissible limit of Pb in drinking water is 0.015 mg/L [4]. Lead concentrations in industrial wastewaters approach 200–500 mg/L; this concentration is very high in water quality standards, and the Pb concentration of wastewaters must be reduced to a level of 0.05–0.10 mg/L before discharging to waterways or sewage systems [5]. Hence, developing efficient purification technologies to remove Pb from water is critically required [6].

Several separation technologies such as membrane process, distillation, electro-dialysis, flotation, photo-catalysis, and chemical coagulation have been applied to remove Pb and other toxic metals from water [7]. Nevertheless, most of these methods show some disadvantages, including excessive operation and maintenance costs, low selectivity, insufficient removal capacity, creating secondary sludge, and persistent requisition for chemicals [8]. Therefore, it is crucial to develop efficient, eco-friendly, and inexpensive treatment methods to remove metals from water. As a highly efficient, easily operated, and affordable technique, adsorption has been extensively used for removing Pb from aqueous solutions [9–11]. Some extensively used adsorbents for the Pb removal include activated carbons [12], clay minerals [13], biomass and lignocellulosic materials [14], industrial byproducts [11], and polymers [15].

Natural and synthetic polymers, containing numerous coordinating groups on their backbones and side-chains, are effective adsorbents for metal removal from water [15]. Polyvinyl alcohol (PVA) is a hydroxyl-rich, non-hazardous, and biodegradable synthetic polymer that strongly interacts with metals [16]. However, pure hydrogels made from PVA are mechanically unstable and should be blended with other polymers or clay fillers to form more mechanically robust hydrogel networks [17]. Alginate (Alg) is a natural, highly hydrophilic biopolymer containing 1,4-linked β-D-mannuronic and α-L-guluronic acid residues [18]. Alginate contains abundant carboxyl groups which can potentially react with polyvalent cations through unidentate or bidentate coordination [19, 20], making it a suitable material for water purification purposes. Nevertheless, the application of Alg-based hydrogels in water treatment practices is limited by their low mechanical strength and high solubility in water [21]. Combination of Alg with PVA forms hydrogels [22] which have been successfully applied for cell immobilization and controlled release of agrochemicals and pharmaceuticals [23–26]. However, Alg/PVA hydrogels have been scarcely used for the adsorptive removal of metal ions from polluted waters. High dissolution rate and weak mechanical strength are potential limitations of PVA/Alg hydrogels for use in water treatment practices. Hence, these hydrogels are often reinforced by various fillers like expandable clays to form nanocomposites [27, 28].

The expandable clay minerals, especially montmorillonite, are usually considered fillers in nanocomposite preparation because of their excellent structural stability, great surface area, non-toxicity, and low cost. Bentonite (BNT) is a geological material that mainly consists of montmorillonite (MMT) clay. The crystal units (layers) of MMT are constituted by an octahedral sheet sandwiched between two tetrahedral sheets. Isomorphic substitution in the octahedral sheet (Mg^{2+} for Al^{3+}) results in an overall negative charge, which is counterbalanced by interlayer cations such as Na^{+}, Ca^{2+}, etc. [29]. BNT has been extensively used to produce clay-polymer nanocomposites, given its outstanding physicochemical properties [30–33]. Strong interfacial interaction between the clay filler and polymer matrix is crucial to obtain the required dispersion of the filler. Hence, surface modification of the clay particles using coupling agents, such as amino acids, is usually performed to introduce functional groups on the clay surfaces, enhancing the interaction between the phases [15].

Recently, nanocomposites containing PVA and BNT exhibit promising results in metal and metalloid removals from water. For example, Wang et al. [33] prepared a chitosan–poly (vinyl alcohol)/bentonite nanocomposite showing a high adsorption capacity for Hg as 460 mg g^{-1}. Baigorria et al. [34] used PVA/Alg hydrogel beads containing natural BNT for As removal from polluted water and showed that clay incorporation played a crucial role in the As removal efficiency. Sanchez et al. [35] also developed novel eco-friendly hydrogel adsorbents based on PVA and an acid-treated BNT. They reported that the presence of acid BNT was beneficial for improving the removal capacity of PVA-based hydrogels. Although considerable studies have been carried out on the different aspects of PVA-clay nanocomposites, there is still a necessity to develop new nanocomposites that possess high adsorption potentials for toxic metals.

In this paper, we prepared and characterized a novel polymer/clay nanocomposite by dispersing a cysteine-modified BNT in a PVA/Alg matrix. The cysteine amino acid modifier was used to functionalize the BNT surface and make it

Table 1 Results of elemental decomposition of natural bentonite sample used in this study

SiO_2	Al_2O_3	Fe_2O_3	CaO	Na_2O	Cl	SO_3	MgO	K_2O	SrO	TiO_2	ZrO_2	MnO	CuO
72.93	10.30	2.28	2.25	2.02	1.39	1.39	1.27	0.38	0.27	0.040	0.029	0.024	0.013

more interactive with PVA and Alg polymers. The synthesized nanocomposite was further utilized for the removal of Pb from aqueous solutions. To the best of our knowledge, no previous research has been conducted using this starting materials' combination to synthesize adsorbent for Pb removal from aqueous solutions.

Materials and Methods

Materials

All applied chemicals were analytical grade, and distilled water was used in all experimental processes. The PVA with a polymerization degree of 1500 (molecular weight: 66,000 g mol^{-1}) and L-cysteine (99%, Mw = 121.15 g mol^{-1}) were supplied by Dae-Jung Chemicals and Metals Co., Korea. Sodium alginate (Alg) was obtained from Sigma–Aldrich with a mannuronate/guluronate ratio of 39/61 and a molecular weight of 120–190 kDa. The natural BNT from the Mehredjan mine (33° 36′ 7″ N, 55° 10′ 4″ E) was applied in the study. The elemental analysis of the BNT sample was performed using X-ray fluorescence spectrometry (XRF) and is represented in Table 1. The cation exchange capacity (CEC) of the BNT was 66.0 cmol kg^{-1} as measured by the ammonium acetate method [36]. A stock solution containing 1000 mg Pb L^{-1} was produced by dissolving $PbNO_3$ (> 99%, Merck) in distilled water and subsequently used for preparing the dilutions.

Surface Modification of BNT with Cysteine

Bentonite (3.0 g., dry basis) was added to 75 mL distilled water and agitated for 2 h at 60 °C. Subsequently, 30 mL of 0.2 M L-cysteine was slowly added to the suspension and stirred for another 3 h. The suspension was centrifuged, and the resulting modified clay (Cys-BNT) was separated using filter paper [37]. Finally, the Cys-BNT was freeze-dried and stored at room temperature.

Synthesis of Cys-BNT/PVA/Alg Nanocomposites

Three grams of PVA and 0.3 g of Na–Alg were mixed with 100 mL distilled water and stirred for 3 h with a magnetic stirrer at 60 °C. After 2 h, 10 mL boric acid 6% was added to the solution for developing chemical bonds between the two polymers. Subsequently, the final solution was undergone a freezing-melting period (24 h under − 20 °C and then 4 h under room temperature) to create a physical bond between these components. Subsequently, a 10% Cys-BNT suspension (10 mL) was added to the PVA/Alg solution and stirred for 2 h. The mixture was then placed at room temperature for 42 h to cause more interaction between the various components. Finally, the produced Cys-BNT/PVA/Alg composite was sediment by adding 100 mL of acetone. The nanocomposite was washed with distilled water, dried at 100 °C for 12 h, and powdered in liquid nitrogen. The same procedure was carried out to prepare the BNT/PVA/Alg composite except that BNT instead of Cys-BNT was used.

Characterization

X-ray diffraction (XRD) analysis was performed using a Philips PW1730, (Philips, Eindhoven, Netherlands) X-ray diffractometer with Cu-Kα radiation ($\lambda = 1.54056$ Å) operated at 40 kV and 30 mA. The data were collected in the 2θ range of 2°–80° with a step size of 0.05° and a counting time per step of 1 s.

Fourier transform infrared (FT-IR) spectra were obtained between 4000 and 400 cm^{-1} on an IR spectrometer (JASCO-680, Tokyo, Japan) using the standard KBr pellet disc technique. Each IR spectrum was an accumulation of 32 scans at a resolution of 4 cm^{-1}.

The morphology of the nanocomposites was observed using a transmission electron microscope (TEM) (Philips, CM120, Eindhoven, Netherland) with an accelerating voltage of 100 kV.

Lead Adsorption Kinetics

To determine the equilibrium time and rate of Pb adsorption on the composites, kinetic experiments were performed. Samples (0.02 g) of the adsorbents were weighed in polyethylene containers in triplicates. Subsequently, 10 mL of a solution containing a Pb concentration of 100 µmol L^{-1} was added to each container. The suspensions were shaken in an incubator shaker (30 °C, 180 rpm) for different time intervals of 0.25 to 9 h. Then, the suspensions were centrifuged for 10 min at 3500 rpm, and the resulting supernatants were analyzed for Pb concentration by atomic absorption spectroscopy (AAS) performed with a Perkin-Elmer AAnalyst 200 model.

The adsorbed Pb per mass unit of the sorbents was calculated according to the following formula:

$$q_t = \frac{(C_0 - C_t)V}{W} \quad (1)$$

Table 2 Kinetic models tested to describe time-dependent Pb adsorption data

Kinetic model	Equation	Nomenclature
Pseudo-first order	$q_t = q_e(1 - e^{-k_1 t})$	q_e and q_t (μmol g^{-1}) are the amounts of the Pb adsorbed at equilibrium and at any time (h), respectively; and k_1 (h^{-1}) is the rate constant of the pseudo-first-order model
Pseudo-second order	$q_t = \frac{k_2 q_e^2 t}{1+k_2 q_e t}$	k_2 (g μmol^{-1} h^{-1}) is the rate constant of the pseudo-second-order equation; q_e (μmol g^{-1}) is the equilibrium adsorption capacity; q_t (μmol g^{-1}) and t (h) were defined above The "initial adsorption rate" (ρ) (μmol g^{-1} h^{-1}) was determined using the parameters of the pseudo-second-order equation as follows: $\rho = k_2 q_e^2$
Elovich	$q_t = \frac{1}{\beta}\ln(\alpha\beta) + (\frac{1}{\beta})\ln t$	α (μmol g^{-1} h^{-1}) and β (g μmol^{-1}) are model constants related to the initial adsorption rate and surface coverage, respectively, and q_t (μmol g^{-1}) and t (h) were defined above
Power function	$q_t = at^b$	a and b are the model constants, and q_t and t were described above. The "ab" function is termed as the "specific adsorption rate at the unit time"
Intra-particle diffusion	$q_t = K_{dif} t^{1/2} + C$	K_{dif} (μmol g^{-1} $h^{-1/2}$) is the intra-particle diffusion rate constant, C is the model intercept, and q_t (μmol g^{-1}) and t (h) were defined above

where q_t is the amount of Pb adsorbed on the adsorbent at time t (μmol g^{-1}), C_0 and C_t are Pb concentrations (μmol L^{-1}) at times 0 and t, respectively, V is the volume of the solution (L), and W is the mass of the adsorbent used (g).

Finally, the pseudo-first-order, pseudo-second-order, Power function, Elovich, and parabolic diffusion models (Table 2) were used to describe the experimental data.

Lead Adsorption Isotherms

Lead adsorption isotherms by PVA/Alg, BNT/PVA/Alg, and Cys-BNT/PVA/Alg composites were determined using the batch method. Samples (0.02 g) of each composite were added to 15 mL of solutions containing Pb with concentrations ranging from 25 to 1200 μmol L^{-1}. The mixtures were shaken for 4 h, as determined in the preliminary kinetic test, in an incubator shaker (30 °C, 180 rpm). A control sample without adsorbent was also considered for each Pb concentration. After equilibration, the suspensions were centrifuged for 10 min at 4500×*g* and the supernatants were separated and analyzed for Pb concentration by the AAS. The adsorbed amount of metal in the systems was calculated according to Eq. 2:

$$q_e = \frac{(C_0 - C_e)V}{W} \quad (2)$$

where q_e is the Pb adsorbed at equilibrium (μmol g^{-1}), C_0 and C_e are Pb concentrations (μmol L^{-1}) at initial and equilibrium conditions, respectively, V is the solution volume (L), and W is the adsorbent mass (g).

The Langmuir and Freundlich models were fitted to the Pb adsorption equilibrium data. The parameters of the isothermal models are described in Table 3.

Table 3 Isothermal equations used to fit the equilibrium Pb adsorption data

Isotherm	Equation	Nomenclature
Langmuir	$q_e = \frac{q_{max} K_L C_e}{1+K_L C_e}$	q_e is the equilibrium Pb concentration adsorbed by the composite (μmol g^{-1}), C_e is the equilibrium Pb concentration in solution (μmol L^{-1}), q_{max} is the Pb adsorption capacity of the composite (μmol g^{-1}), and K_L is the Langmuir constant (L μmol^{-1}) related to the adsorption energy
Freundlich	$q_e = K_F C_e^N$	K_F (μmol^{1-n} L^n g^{-1}) is the Freundlich constant relating to the adsorption capacity and N is a coefficient showing adsorption strength and surface heterogeneity. The q_e and C_e were defined above

Effect of pH on Pb Removal

The Pb adsorption experiments were carried out at different pH values to determine the optimum range for Pb adsorption. For this purpose, 15 mL of Pb solution (97 μmol L^{-1}) and 0.02 g adsorbent were added to each container. Afterward, the pH values of the suspensions were adjusted from 2 to 7 either by 0.1 M HCl or 0.1 M NaOH before they were shaken in an incubator-shaker for 4 h. The suspensions were then centrifuged for 10 min at 3500 rpm and passed through a filter paper. Finally, the Pb concentration in the solution was measured by the AAS.

The PHREEQC geochemical model (version 2.18.00) was applied to estimate the dominant Pb species in solutions. The saturation index (*SI*) was also calculated according to Eq. (3), to determine if the solutions were supersaturated with respect to the Pb minerals:

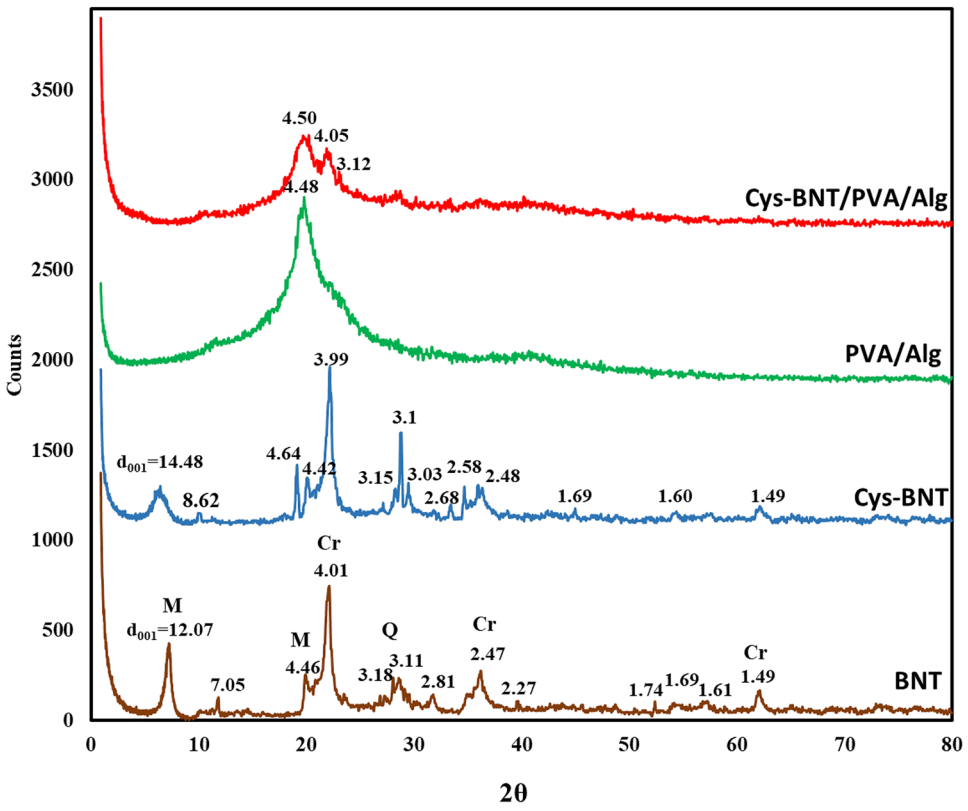

Fig. 1 X-ray diffraction patterns of natural bentonite (BNT), cysteine-bentonite (Cys-BNT), poly (vinyl alcohol)/alginate (PVA/Alg) composite, and cysteine-bentonite/poly (vinyl alcohol)/alginate nanocomposites (Cys-BNT/PVA/Alg) (*M* montmorillonite, *Cr* cristobalite, *Q* quartz)

$$SI = \log\left(\frac{IAP}{K_{sp}}\right) \tag{3}$$

where IAP is the ion activity product and K_{sp} is the solubility product constant of the mineral. A negative SI value indicates under-saturation, while a positive one represents super-saturation, with respect to a given mineral.

Model Fitting and Statistical Analysis

Kinetic and isothermal models were fitted to the Pb adsorption data using the nonlinear regression method in Graphpad Prism 8.4.2 software (GraphPad Software, Inc., CA, USA). The goodness-of-fit of the models for describing the Pb adsorption data was assessed using the determination coefficients (R^2), and the standard errors of estimate (SEE) were calculated as follows:

$$SEE = \left[\frac{\sum (q - q')}{n - 2}\right]^{1/2} \tag{4}$$

where q and q' are measured and predicted Pb adsorbed values, respectively, and n is the number of measurements.

Statistical comparison between the model parameters was performed using the extra sum-of-squares F test in Graphpad Prism 8.4.2 (GraphPad Software, Inc., CA, USA).

Results and Discussion

X-ray Diffraction Patterns

Figure 1 represents the XRD diffractograms of the composites prepared in this study. The XRD pattern of the PVA/Alg composite exhibited only one broad peak at 2θ = 19.5°. This peak corresponds to the semicrystalline PVA structure, consistent with previous reports [38–40].

Figure 1 also shows that the raw BNT sample mainly consisted of montmorillonite (MMT), quartz (QTZ), and cristobalite (CST). The MMT characteristic peak was observed at 2θ = 7.25°, attributed to basal spacing (d 001) of 1.21 nm, which is consistent with a Na-MMT. The diffraction peak of MMT shifted to a lower 2θ value of 6.09° as a result of the clay treatment with Cys (Fig. 1), which indicates that the basal spacing of MMT was increased to 1.45 nm due to the intercalation of Cys molecules into the MMT layers. This weakens attractive forces and lowers the energy barrier needed to exfoliate the clay lamellae into the polymer matrix. The results are consistent with that reported by Öztürk et al. [37], showing that the Cys molecules diffused into the BNT interlayers spaces as the d001 peak shifted from 1.27 nm to 1.40 nm after Cys intercalation. Ahmad and Mirza [30] also reported that L-methionine amino acid successfully penetrated the MMT internal spaces and increased

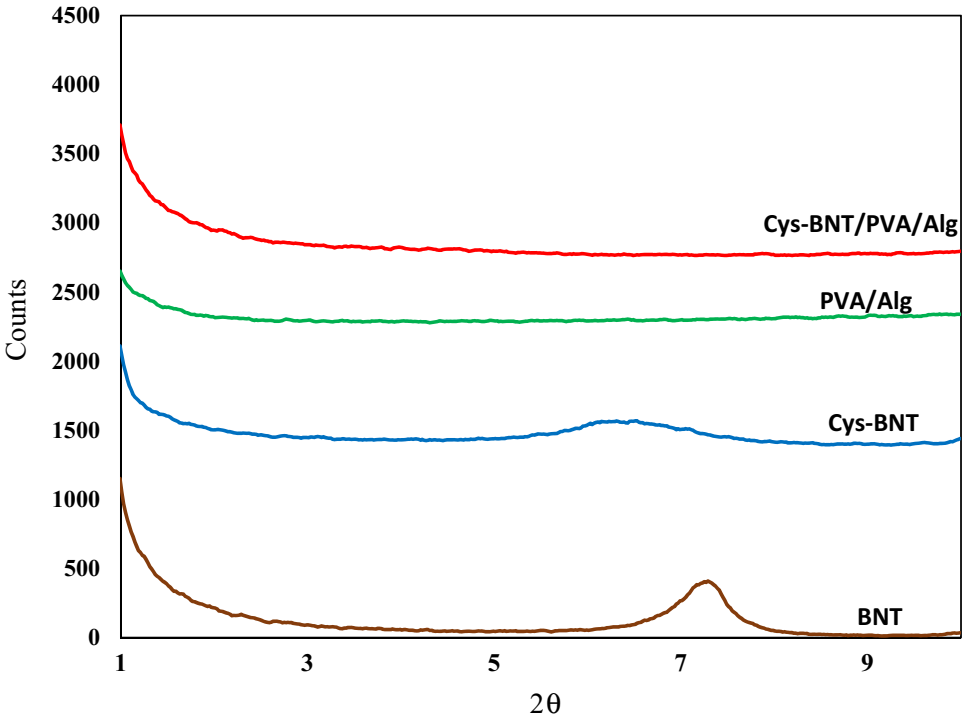

Fig. 2 Low angle X-ray diffraction patterns of natural bentonite (BNT), cysteine-bentonite (Cys-BNT), poly (vinyl alcohol)/alginate (PVA/Alg) composite, and cysteine-bentonite/poly (vinyl alcohol)/alginate nanocomposites (Cys-BNT/PVA/Alg)

the distance between the clay layers, as revealed by an XRD analysis.

The XRD analysis was used to investigate the exfoliation/intercalation of the clay in the polymer matrix. Based on the wide angle (Fig. 1) and the low angle (Fig. 2) XRD diffractograms, the d_{001} diffraction peak on the XRD pattern corresponding to basal spacing of MMT disappeared for the Cys-BNT/PVA/Alg nanocomposite, suggesting that the parallel arrangement of the clay layers was not maintained due to the exfoliation of clay layers within the PVA/Alg matrix. Jose et al. [41] reported that BNT nanoclays were intercalated in the PVA matrix at lower concentrations and exfoliated at higher concentrations. Exfoliation of BNT in *kappa*-carrageenan/PVA and chitosan/PVA composites have also been reported by Hosseinzadeh et al. [42] and Wang et al. [33], respectively. Nevertheless, Morgan and Gilman [43] stated that the absence of a peak is not proof of exfoliation, and the configuration of the clay within the polymer should be confirmed using TEM techniques.

The PVA characteristic peak at $2\theta = 19.5°$ was broader in the Cys-BNT/PVA/Alg diffractogram than in the PVA/Alg diffractogram, indicating the crystallinity of the PVA polymer reduced with the clay addition.

TEM Images

TEM analysis was adopted to further validate and confirm the structure, which was presumed through XRD measurements. The TEM images of the Cys-BNT/PVA/Alg nanocomposite is shown in Fig. 3. The images showed regions where intercalated tactoids of clay present. However, in some parts, the bentonite layers are discrete and dispersed within the polymer matrix accompanied by the formation of exfoliated structure, which was confirmed by the XRD analysis. Hence, a nanocomposite with a mixture of intercalated and exfoliated microstructures was formed. Using XRD and TEM techniques, Hosseinzadeh et al. [42] also showed that both intercalated and exfoliated structures of κ-carrageenan/poly(vinyl alcohol) nanocomposite hydrogel were produced after montmorillonite incorporation. Generally, a completely exfoliated structure on a polymer–clay nanocomposite is scarce and difficult to obtain, and the majority of the nanocomposites have mixed structures [44].

FT-IR Spectra

The FT-IR spectra of BNT, Cys-BNT, PVA/Alg, BNT/PVA/Alg, and Cys-BNT/PVA/Alg are shown in Fig. 4. The peaks at 3434 cm^{-1} and 3630 cm^{-1} were assigned to asymmetric stretching vibrations of O–H in the Si–OH and Al–OH groups of the MMT, and water molecules, respectively [45–47]. The peak at 1638 cm^{-1} can be related to the bending of OH groups in water molecules [48]. The bands at 1087 cm^{-1} and 1041 cm^{-1} are related to Si–O–Si or Si–O stretching in the bentonite structure. The characteristic bands at 795 cm^{-1}, 621 cm^{-1}, 518 cm^{-1}, and 469 cm^{-1} are related to Si–O in quartz and silica structures, Al–O and

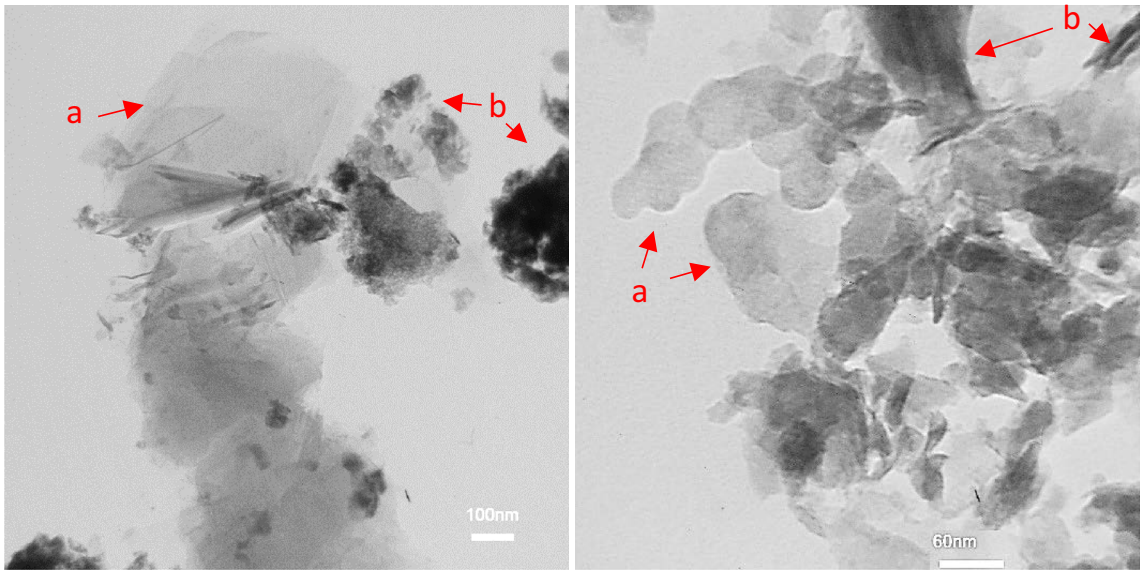

Fig. 3 Transmission electron microscopes (TEM) images of the cysteine-bentonite/poly (vinyl alcohol)/alginate (Cys-BNT/PVA/A) nanocomposites at two different magnifications. **a** Exfoliated single layers and **b** small intercalated clay tactoids were present

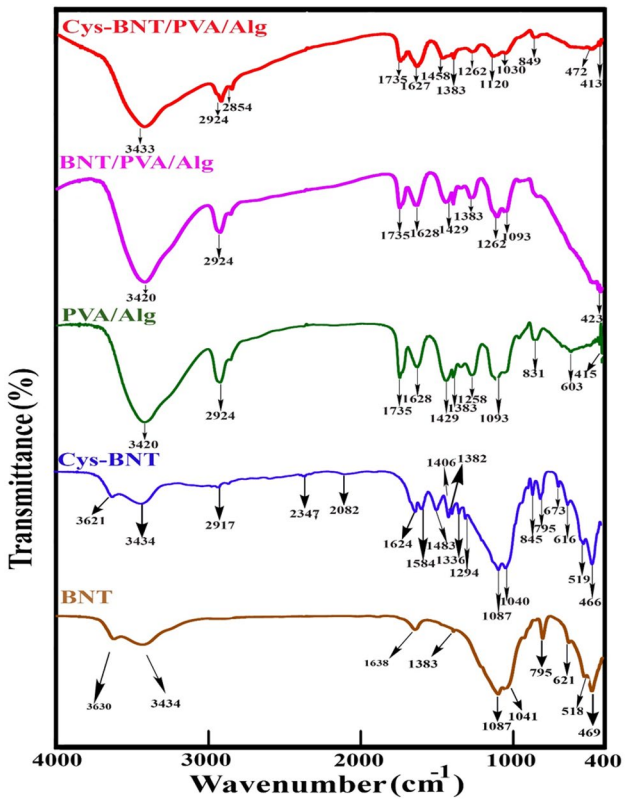

Fig. 4 FT-IR spectra of the natural bentonite (BNT), cysteine-bentonite (Cys-BNT), poly (vinyl alcohol)/alginate (PVA/Alg) composites, bentonite/poly (vinyl alcohol) composites/Alginate (BNT/PVA/Alg), and cysteine-bentonite/poly (vinyl alcohol)/alginate (Cys-BNT/PVA/A) nanocomposite

Si–O out-of-plane vibration, Si–O–Al bending, and Si–O–Si bending, respectively [41].

The modification of BNT with cysteine noticeably changed the FT-IR spectrum of BNT (Fig. 4). For instance, several new bands in the 2900–3420 cm^{-1} range correspond to the $–NH_2$ group, 1550–1600 cm^{-1} range, and 1382 cm^{-1} related to $–COO^-$ group, 1294 cm^{-1} associated with C–H bending, and 600–800 cm^{-1} range attributed to C–S groups [49, 50] appeared on FT-IR spectrum of BNT after Cy's adsorption. The existing IR absorption bands of $–COO^-$ and $–NH_2$ in the Cys-BNT spectrum confirm that the surface modification of the BNT by Cys was successfully achieved.

The FT-IR spectrum of the PVA/Alg composite shows the characteristic peak of –OH in the 1350–3550 cm^{-1}, which is attributed to the OH stretching vibration of the intermolecular and intramolecular hydrogen bindings [51]. The band at 2924 cm^{-1} is related to the symmetric, and asymmetric stretching vibrations of the CH_2 group, and the one at 1735 cm^{-1} is associated with the acetate groups from polyvinyl acetate [52]. The peak at 1628 cm^{-1} can be attributed to symmetrical vibration or deformation of H–OH. The 1429 and 1383 cm^{-1} bands are attributed to the vibrations of the C–H groups. The symmetric stretching vibration of –COOH has also been reported at this wavenumber [53]. The band centered at 1258 cm^{-1} is related to the symmetric C–C or C–O stretching as a part of the polymer chain [52, 54]. The peak at 1093 cm^{-1} is due to, C–O and O–H stretching and C–H deformation in PVA/Alg composite [55]. The band at 831 cm^{-1} is related to $–CH_3$ vibration, and that at 603 cm^{-1} is assigned to C–C–O and C–C–H groups. The

peak of 415 cm^{-1} can be attributed to the vibration of the C–OH bond.

When BNT was added to the PVA/Alg composite, some changes occurred in the IR spectrum. For example, the 1258 cm^{-1} peak shifted to 1262 cm^{-1}, the 415 cm^{-1} peaks moved to 423 cm^{-1}, and the 831 and 603 cm^{-1} peaks disappeared, reflecting the interaction between PVA/Alg and clay particles.

When Cys-BNT was added to the PVA/Alg composite, the peak at 3420 cm^{-1} was shifted to 3434 cm^{-1}, probably due to increased hydrogen bonding in the Cys-BNT/PVA/Alg in the presence of the –NH groups of the Cys amino acid. Incorporation of Cys–BNT eliminated the peak at 1429 cm^{-1} in the PVA/Alg spectrum related to vibration of the C–H bands. The peak at 1429 cm^{-1} in the PVA/Alg spectrum related to vibration of the C–H bands was eliminated after the incorporation of Cys–BNT. Instead, a band at 1458 cm^{-1} appeared in the Cys-BNT/PVA/Alg spectrum, which may be related to the NH-induced vibration caused by the presence of Cys-BNT. Moreover, the peak at 1903 cm^{-1} in the PVA/Alg composite shifted to 1120 cm^{-1} in the presence of Cys-BNT, and its intensity decreased consequently (Fig. 4). This peak may be due to the presence of C–N, indicating a proper interaction of Cys-BNT and PVA/Alg. Also, the peak at 831 cm^{-1} was shifted to 849 cm^{-1}, and its intensity decreased, which can be attributed to the $–CH_3$ and C–S band vibrations [56]. Moreover, in the spectrum of this nanocomposite, the peak of 603 cm^{-1} disappeared.

Lead Adsorption Isotherms

The Langmuir and Freundlich isotherm constants, determination coefficients, and standard errors of estimates are listed in Table 4. The results indicate that both models adequately explained the experimental data, but the Langmuir model fits the equilibrium data better (Table 4, Fig. 5). Shooto et al. [57] and Ren et al. [58] also successfully used the Langmuir model to describe Pb adsorption on poly (vinyl alcohol) hydrogel strengthened with nanofibers and alginate/carboxymethyl cellulose gel, respectively. Similarly, adsorption of heavy metals by poly (vinyl alcohol)/carboxymethyl starch-grafted poly(vinyl imidazole) composite beads obeyed the Langmuir equation [59].

The maximum Pb adsorption capacity (q_{max}) of PVA/Alg, BNT/PVA/Alg, and Cys-BNT/PVA/Alg composites were 480, 724, and 995 µmol g^{-1}, respectively, indicating a significant improvement in Pb adsorption potential of PVA/Alg hydrogel after modification by BNT and particularly Cys-BNT. The Freundlich K_F parameter, an adsorption capacity factor, also increased from 578 for the PVA/Alg to 979 and 1395 for the BNT/PVA/Alg and Cys-BNT/PVA/Alg, respectively (Table 4). The increased Pb sorption capacity of PVA/Alg after BNT addition is probably due to the development of new sorption surfaces as a result of the expansion or exfoliation of the MMT layers. The more significant role of Cys-BNT than BNT in enhancing the sorption capacity of PVA/Alg hydrogel might be due to the higher surface functional groups of Cys-BNT, as confirmed by FT-IR analysis. Faghihian and Nejati-Yazdinejad [60] also found that the Pb adsorption capacity of Cys-BNT was higher than that of natural BNT. Table 5 compares the Pb sorption capacities of various polymer-based composites reported in previous articles with those of the Cys-BNT/PVA/Alg and BNT/PVA/Alg composites attained in this study. Even though it is somewhat rough to compare the sorption capacities obtained under dissimilar experimental setups, the Cys-BNT/PVA/Alg synthesized in the current study has a relatively high Pb sorption capacity.

Table 4 Constants, determination coefficients (R^2), and standard errors of estimates (*SSE*) resulted from fitting Langmuir and Freundlich models to the lead adsorption data on the poly(vinyl alcohol)/alginate (PVA/Alg), bentonite/poly(vinyl alcohol/alginate (BNT/PVA/Alg) and cysteine-bentonite/poly (vinyl alcohol)/alginate (Cys-BNT/PVA/Alg) adsorbent

Model parameter	Adsorbent		
	PVA/Alg	BNT/PVA/Alg	Cys-BNT/PVA/Alg
Langmuir			
q_{max} (µmol g^{-1})	480.3^{c}	724.3^{b}	995.1^{a}
K_L (L µmol^{-1})	20.85^{a}	16.50^{b}	9.760^{c}
R^2	0.990	0.994	0.979
SEE	17.27	18.78	39.64
Freundlich			
K_F (µmol^{1-N} L^N g^{-1})	578.5^{c}	979.1^{b}	1395^{a}
N	0.360^{c}	0.426^{b}	0.501^{a}
R^2	0.913	0.937	0.948
SSE	50.61	59.58	61.90

The Langmuir K_L constant was 20.85, 16.50, and 9.76 L $mmol^{-1}$ for the PVA/Alg, BNT/PVA/Alg, and Cys-BNT/PVA/Alg samples, respectively, indicating that the overall affinity of the PVA/Alg active sites for Pb binding is higher than those of the BNT/PVA/Alg, and Cys-BNT/PVA/Alg. The value of the Freundlich *N* parameter was 0.36 for PVA/Alg, which increased to 0.42 and 0.50 after the incorporation of BNT and Cys-BNT (Table 4), confirming that PVA/Alg functional groups form stronger bonds with Pb ions as the smaller Freundlich *N* parameter suggests the formation of stronger bonds [61].

Effect of pH on Pb Removal

The solution pH is a significant factor regulating the adsorption of heavy metals. The impact of solution pH on Pb

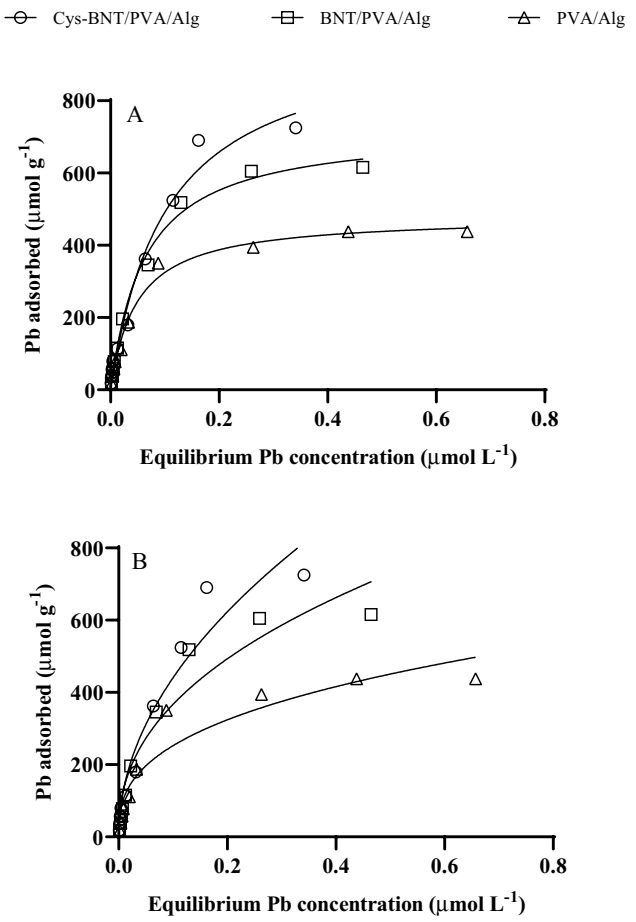

Fig. 5 Lead adsorption isotherms of the poly (vinyl alcohol)/alginate (PVA/Alg), bentonite/poly (vinyl alcohol)/alginate (BNT/PVA/Alg), and cysteine-bentonite/poly (vinyl alcohol)/alginate (Cys-BNT/PVA/A) composites fitted by the Longmuir (**a**) and Freundlich (**b**) models. (T: 30 °C; sorbent dosage, 1.33 g L^{-1}; agitation speed: 180 rpm; contact time: 4 h; C_0: 25 to 1200 μmol Pb L^{-1})

adsorption was explored by ranging the pH value of the metal solution from 2.0 to 7.0. The results showed that the adsorption was maximum at pH 5.0 and decreased as the solution pH was raised or lowered (Fig. 6). The maximum removal efficiency of Pb ions by the PVA/Alg, BNT/PVA/Alg, and Cys-BNT/PVA/Alg composites at the optimum pH value were about 50%, 61%, and 75%, respectively. Free Pb^{2+} ions were the dominated Pb species in solutions in the pH range of 2–7 (Table 6). At the low pH values, the H^+ concentration is far higher than that of the Pb ions; therefore H^+ ions compete with the Pb ions for chemisorption on the surface functional groups [62, 63]. Moreover, the protonation of amino groups on the composite surfaces produces positive charges, preventing the metal cations from moving toward the adsorbent surface through repulsive forces [64]. Formation of hydrolyzed species $Pb(OH)^+$ and Pb precipitate ($Pb(OH)_2$), as revealed from speciation calculations (Table 6), could be possible factors reducing the Pb removal efficiency past the optimum pH value [65]. Anitha et al. (2015) also found that the maximum removal of Pb by poly (vinyl alcohol)/chitosan was obtained at pH 5. The same pH values were also reported by Jamnongkan et al. [66] as the optimum pH value for Cu removal by poly (vinyl alcohol) hydrogels.

Kinetics of Pb Removal

The Pb adsorption process by the composites was rapid and reached equilibrium in almost 4 h (Fig. 7). The fast adsorption might be due to plenty of high-energy empty sites accessible for binding Pb ions, which give rise to immediate Pb adsorption. Over 60% of the Pb adsorption occurred within the first hour, indicating a high binding affinity between Pb ions and active sites on the composite surfaces. The available active sites on the composites were gradually occupied over time, and the adsorption rate gradually decreased. Abraham et al. [67] reported the equilibrium time of 8 h for Pb adsorption by Poly (vinyl alcohol)-based MWCNT hydrogel.

The time-dependent Pb adsorption onto the composites significantly ($P < 0.01$) fitted by the pseudo-first-order, pseudo-second-order, Elovich, power function, and intraparticle diffusion models. The Elovich model was superior in describing the kinetic data according to the R^2 values presented in Table 7. Based on the kinetic results, incorporation of Cys-BNT significantly ($P < 0.05$) increased the amount and rate of Pb adsorption by the PVA/Alg hydrogel, while the increases induced by BNT addition were not statistically significant at $P < 0.05$ (Table 7).

The determination coefficients for the first-order kinetic model were 0.69–0.90 (Table 7). The calculated q_{e1} values were 29.7, 30.3, and 33.5 mmol kg^{-1} for the PVA/Alg, BNT/PVA/Alg, and Cys-BNT/PVA/Alg composites, respectively, which agreed well with the experimentally measured Pb adsorption at equilibrium. The Pb adsorption rate constant k_1 was found to be 0.917, 1.088, and 1.552 h^{-1} for the PVA/Alg, BNT/PVA/Alg, and Cys-BNT/PVA/Alg, respectively (Table 7), indicating the shortest Pb adsorption reaction time on Cys-BNT/PVA/Alg if a fixed amount of Pb is present in the system.

The pseudo-second-order parameters, qe_2 and k_2, obtained from the pseudo-second-order plots are presented in Table 7. The R^2 values (0.84–0.95) were higher compared to those of the pseudo-first-order model. The estimated q_{e2} values (34.0, 34.2, and 36.9 mmol kg^{-1} for PVA/Alg, BNT/PVA/Alg, and Cys-BNT/PVA/Alg, respectively) also agree with the results obtained from the pseudo-second-order kinetics. The k_2 value increased from 0.035 for PVA/Alg to 0.044 and 0.062 g μmol^{-1} h^{-1} for the BNT/PVA/Alg and Cys-BNT/PVA/Alg, respectively. The calculated initial Pb adsorption rates (ρ) for the PVA/

Table 5 Comparison of Pb adsorption capacity of the poly(vinyl alcohol)/alginate/Cysteine-bentonite and poly(vinyl alcohol)/alginate/bentonite composites obtained in the present research and those of different polymer matrix composites reported in the literature

Adsorbent	Adsorption capacity (μmol g^{-1})	References
Cysteine-bentonite/poly(vinyl alcohol)/alginate	995.1	Current work
Bentonite/poly(vinyl alcohol)/alginate	724.3	Current work
Polypyrrole/multi-walled carbon nanotube	120.6	[70]
Polypyrrole (PPy)/silica	530.4	[71]
Polypyrrole coated oxidized multiwalled carbon nanotubes	127.0	[72]
Carboxymethyl-β-cyclodextrin modified Fe_3O_4	311.3	[73]
Polyaniline nanofibers coated millimeter-scale calcium alginate gel	1212	[74]
poly(ethyleneimine)-silica gels	398.8	[75]
poly(aniline-*co*-3-aminobenzoic acid)-based magnetic core–shell	667.5	[76]
Polyvinyl butyral/potassium polytitanate	661.2	[77]
Poly-methacrylic acid grafted chitosan-bentonite	535.7	[78]

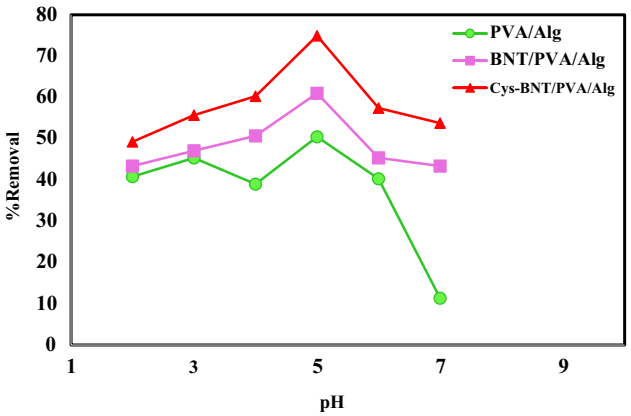

Fig. 6 Effect of pH on Pb removal by the poly (vinyl alcohol)/alginate (PVA/Alg), bentonite/poly (vinyl alcohol)/alginate (BNT/PVA/Alg), and cysteine-bentonite/poly (vinyl alcohol)/alginate (Cys-BNT/PVA/Alg)

Alg were 41.0 μmol g^{-1} h^{-1} which increased to 51.1 and 83.9 μmol g^{-1} h^{-1} after incorporation of BNT and Cys-BNT, respectively.

The Elovich model fitted the Pb adsorption better than the pseudo-first-order, and the pseudo-second-order models with R^2 values ranged from 0.91 to 0.95 (Table 7). The Elovich α and β constants, related to the initial adsorption rate and surface coverage, respectively [68], were found to increase with the addition of BNT and Cys-BNT to the PVA/Alg. Therefore, the incorporation of BNT and Cys-BNT increased the rate of Pb adsorption as well as the available adsorption surface for Pb ions (Table 7). However, only the enhancing effects of Cys-BNT were statistically significant ($P < 0.05$).

The power function model was also able to describe the adsorption kinetics of Pb by all adsorbents and was the best-fitted model for BNT/PVA/Alg nanocomposite Pb adsorption kinetic data (Table 7). The addition of BNT

Table 6 The dominant soluble Pb species and saturation indices (*SI*) with respect to $Pb(OH)_2$ in solutions of different pH values equilibrated with the composites as calculated by PHREEQC speciation program. Values in parentheses represent the percentage of total soluble Pb

Composite		pH 2	3	4	5	6	7
PVA/Alg	Dominant species	Pb^{2+} (100%)	Pb^{2+} (100%)	Pb^{2+} (100%)	Pb^{2+} (100%)	Pb^{2+} (98.2%)	Pb^{2+} (84.9%)
						$Pb(OH)^+$ (1.73%)	$Pb(OH)^+$ (14.5%)
	SI $Pb(OH)_2$	− 7.88	− 5.77	− 3.70	− 1.78	0.28	2.46
BNT/PVA/Alg	Dominant species	Pb^{2+} (100%)	Pb^{2+} (100%)	Pb^{2+} (100%)	Pb^{2+} (100%)	Pb^{2+} (98.1%)	Pb^{2+} (84.7%)
						$Pb(OH)^+$ (1.74%)	$Pb(OH)^+$ (15.0%)
	SI $Pb(OH)_2$	− 7.73	− 5.69	− 3.69	− 1.79	0.24	2.20
Cys-BNT/PVA/Alg	Dominant species	Pb^{2+} (100%)	Pb^{2+} (100%)	Pb^{2+} (100%)	Pb^{2+} (100%)	Pb^{2+} (98.2%)	Pb^{2+} (84.5%)
						$Pb(OH)^+$ (1.74%)	$Pb(OH)^+$ (14.9%)
	SI $Pb(OH)_2$	− 7.78	− 5.75	− 3.82	− 1.97	0.23	2.21

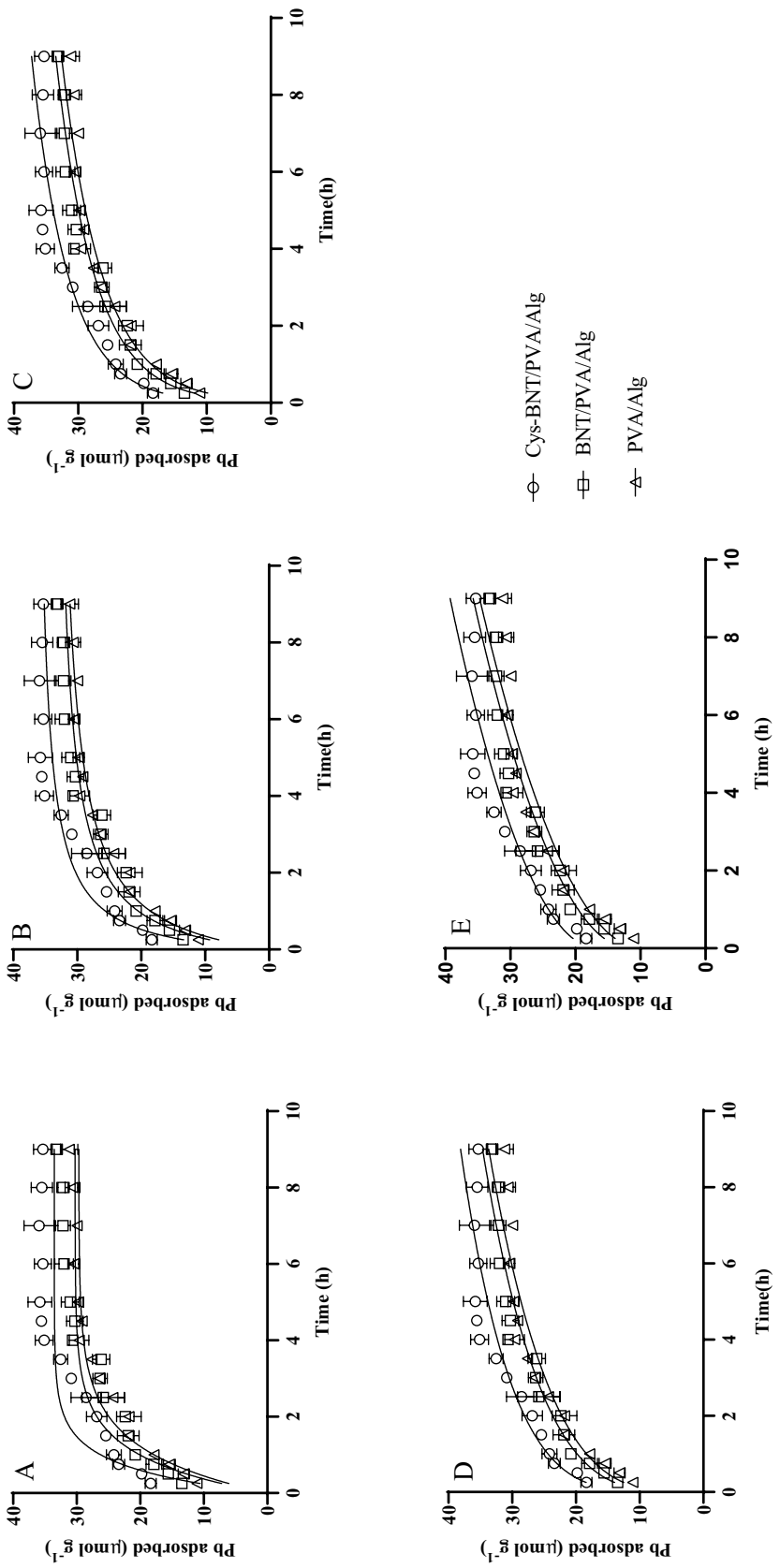

Fig. 7 Time-dependent Pb adsorption data of the poly (vinyl alcohol)/alginate (PVA/Alg), bentonite/poly (vinyl alcohol)/alginate (BNT/PVA/Alg), and cysteine-bentonite/Poly (vinyl alcohol)/alginate (Cys-BNT/PVA/Alg) composites fitted by the pseudo-first-order (**A**), pseudo-second-order (**B**), Elovich (**C**), power function (**D**), and parabolic diffusion (**E**) models. (T: 30 °C; sorbent dosage, 2 g L^{-1}; agitation speed: 180 rpm; contact time: 0.25 to 9 h; C_0: 100 µmol Pb L^{-1})

Table 7 Constants, determination coefficients (R^2), and standard errors of estimates (*SSE*) for the kinetic models fitted to the lead adsorption data on the poly(vinyl alcohol)/alginate (PVA/Alg), bentonite/poly(vinyl alcohol/alginate (BNT/PVA/Alg) and cysteine-bentonite/poly(vinyl alcohol)/alginate (Cys-BNT/PVA/Alg) adsorbents

Model parameter	Adsorbent		
	PVA/Alg	BNT/PVA/Alg	Cys-BNT/PVA/Alg
Pseudo first order			
q_e (μmol g^{-1})	29.70[b]	30.28[b]	33.55[a]
k_1 (h^{-1})	0.917[b]	1.088[b]	1.522[a]
R^2	0.905	0.779	0.678
SEE	2.080	3.030	3.523
Pseudo second order			
q_e (μmol g^{-1})	34.02[b]	34.20[b]	36.91[a]
k_2 (g μmol^{-1} h^{-1})	0.0354[b]	0.0437[b]	0.0616[a]
h (μmol g^{-1} h^{-1})	40.97 [b]	51.11 [ab]	83.92[a]
R^2	0.952	0.890	0.842
SEE	1.486	2.136	2.465
Elovich			
α (μμmol g^{-1} h^{-1})	119.5[c]	175.5[b]	437.8[a]
β (g μmol^{-1})	0.1572[b]	0.1661[b]	0.1753[a]
R^2	0.953	0.939	0.909
SEE	1.457	1.594	1.868
Power function			
a	18.35[c]	19.84[b]	24.41[a]
b	0.2766[a]	0.2540[a]	0.2030[b]
ab (μmol g^{-1} h^{-1})	5.075[a]	5.039[a]	4.955[a]
R^2	0.927	0.937	0.904
Parabolic diffusion			
K_{dif} (μmol g^{-1} $h^{-1/2}$)	8.336[a]	8.068[a]	7.562[a]
C	9.745[c]	11.55[b]	16.61[a]
R^2	0.881	0.907	0.860
SEE	2.330	1.962	2.323

All R^2 values are significant at $P < 0.01$

Different letters in the same row denote a statistically significant difference ($P < 0.05$)

and Cys-BNT to the PVA/Alg composite significantly increased the specific Pb adsorption rate at the unit time (ab).

Finally, the kinetic data were adequately ($R^2 = 0.86$–0.91) described by the Weber and Morris intraparticle diffusion model (Table 7). The calculated intraparticle diffusion coefficient (k_{dif}) and intercept (C) constants for the Pb sorption on the composites are listed in Table 7. The C constant, which reflects the boundary layer effect, significantly ($P < 0.05$) increased from 9.7 for the PVA/Alg to 11.5 and 16.6 for the BNT/PVA/Alg and Cys-BNT/PVA/Alg, respectively, suggesting a higher contribution of surface adsorption reactions in the rate-controlling step in Pb retention after modification of the PVA/Alg by BNT and Cys-BNT [69].

Conclusions

A poly(vinyl alcohol) (PVA)/alginate (Alg) hydrogel containing cysteine-functionalized bentonite (Cys-BNT) was developed, characterized, and evaluated as a potential device for Pb removal from aqueous solutions. Morphological studies using TEM revealed the excellent dispersion of the clay particles into the polymer matrix, producing both exfoliated and intercalated regions. These results agree well with those obtained in the XRD analysis.

The synthesized nanocomposite was successfully used for Pb removal from aqueous solutions. The incorporation of Cys-BNT caused a significant increase in both the capacity and the rate of Pb adsorption by the PVA/Alg hydrogel. The Cys-BNT/PVA/Alg nanocomposite showed a high Pb adsorption capacity of 995 μmol g^{-1} in a short equilibrium time. The estimated maximum adsorption capacity of the nanocomposite was considerably higher than those of many polymer-based composite adsorbents reported in the literature. Therefore, the synthesized Cys-BNT/PVA/Alg nanocomposite can be effectively used as a suitable adsorbent material for effective and fast removal of Pb from aqueous solutions.

Funding This research was funded by the Isfahan University of Technology.

Data Availability The data are available from the corresponding author on request.

Code Availability No special code was applied in the study.

Declarations

Conflict of interest The authors declare that they have no known competing financial interests or personal relationships that could have appeared to influence the work reported in this paper.

Consent to Participate This research did not involve human participants, identifiable human data, or human tissue.

Consent for Publication This research did not involve human participants, identifiable human data, or human tissue.

Ethical Approval No animals or human participants, their data, or biological materials were included in the study.

References

1. Jayaswal K, Sahu V, Gurjar BR (2018) Water pollution, human health and remediation. In: Bhattacharya S, Gupta AB, Gupta A, Pandey A (eds) Water remediation. Springer, Singapore, pp 11–27

2. RoyChowdhury A, Datta R, Sarkar D (2018) Heavy metal pollution and remediation. In: Török B, Dransfield T (eds) Green chemistry. Elsevier, Amsterdam, pp 359–373
3. Schweitzer L, Noblet J (2018) Chapter - water contamination and pollution. In: Török B, Dransfield T (eds) Green chemistry. Elsevier, Amsterdam, pp 261–290
4. EPA U (2003) Environmental Protection Agency: National primary and secondary drinking water standard. Office of Water (4606M), EPA 816-F-03
5. Arbabi M, Hemati S, Amiri M (2015) Removal of lead ions from industrial wastewater: A review of Removal methods. Int J Epidemiol Res 2:105–109
6. Pereira CP, Goldenstein JPN, Bassin JP (2022) Industrial wastewater contaminants and their hazardous impacts. In: Selvasembian R, Singh P (eds) Biosorption for wastewater contaminants. Wiley, Pondicherry, pp 1–22
7. Bolisetty S, Peydayesh M, Mezzenga R (2019) Sustainable technologies for water purification from heavy metals: review and analysis. Chem Soc Rev 48:463–487
8. Vardhan KH, Kumar PS, Panda RC (2019) A review on heavy metal pollution, toxicity and remedial measures: current trends and future perspectives. J Mol Liq 290:111197
9. Gupta VK, Sharma S (2003) Removal of zinc from aqueous solutions using bagasse fly ash: a low cost adsorbent. Ind Eng Chem Res 42:6619–6624
10. Joseph L, Jun B-M, Flora JRV, Park CM, Yoon Y (2019) Removal of heavy metals from water sources in the developing world using low-cost materials: a review. Chemosphere 229:142–159
11. Singh NB, Nagpal G, Rachna SA (2018) Water purification by using adsorbents: a review. Environ Technol Innov 11:187–240
12. Periyasamy S, Kumar IA, Viswanathan N (2020) Activated carbon from different waste materials for the removal of toxic metals. In: Naushad M, Lichtfouse E (eds) Green materials for wastewater treatment. Springer International Publishing, Cham, pp 47–68
13. Uddin MK (2017) A review on the adsorption of heavy metals by clay minerals, with special focus on the past decade. Chem Eng J 308:438–462
14. Salman M, Athar M, Farooq U (2015) Biosorption of heavy metals from aqueous solutions using indigenous and modified lignocellulosic materials. Rev Environ Sci Biotechnol 14:211–228
15. Rivas BL, Sánchez J, Urbano BF (2016) Polymers and nanocomposites: synthesis and metal ion pollutant uptake. Polym Int 65:255–267
16. Wang L-Y, Wang M-J (2016) Removal of heavy metal ions by poly(vinyl alcohol) and carboxymethyl cellulose composite hydrogels prepared by a freeze-thaw method. ACS Sustain Chem Eng 4:2830–2837
17. Kumar A, Han SS (2017) PVA-based hydrogels for tissue engineering: A review. Int J Polym Mater Polym Biomater 66:159–182
18. Wang B, Wan Y, Zheng Y, Lee X, Liu T, Yu Z, Huang J, Ok YS, Chen J, Gao B (2019) Alginate-based composites for environmental applications: a critical review. Crit Rev Environ Sci Technol 49:318–356
19. Attar K, Demey H, Bouazza D, Sastre MA (2019) Sorption and desorption studies of Pb(II) and Ni(II) from aqueous solutions by a new composite based on alginate and magadiite materials. Polymers 11:340
20. Papageorgiou SK, Kouvelos EP, Favvas EP, Sapalidis AA, Romanos GE, Katsaros FK (2010) Metal–carboxylate interactions in metal–alginate complexes studied with FTIR spectroscopy. Carbohydr Res 345:469–473
21. Hajiali H, Heredia-Guerrero JA, Liakos I, Athanassiou A, Mele E (2015) Alginate nanofibrous mats with adjustable degradation rate for regenerative medicine. Biomacromol 16:936–943
22. Shen W, Hsieh Y-L (2014) Biocompatible sodium alginate fibers by aqueous processing and physical crosslinking. Carbohydr Polym 102:893–900
23. Flórez-Castillo JM, Ropero-Vega JL, Perullini M, Jobbágy M (2019) Biopolymeric pellets of polyvinyl alcohol and alginate for the encapsulation of Ib-M6 peptide and its antimicrobial activity against *E. coli*. Heliyon 5:01872
24. Kamoun EA, Kenawy E-RS, Tamer TM, El-Meligy MA, Mohy Eldin MS (2015) Poly (vinyl alcohol)-alginate physically crosslinked hydrogel membranes for wound dressing applications: characterization and bio-evaluation. Arab J Chem 8:38–47
25. Russo R, Giuliani A, Immirzi B, Malinconico M, Romano G (2004) Alginate/Polyvinylalcohol Blends for Agricultural Applications: Structure-Properties Correlation, Mechanical Properties and Greenhouse Effect Evaluation. Macromol Symp 218:241–250
26. Şanlı O, Ay N, Işıklan N (2007) Release characteristics of diclofenac sodium from poly(vinyl alcohol)/sodium alginate and poly(vinyl alcohol)-grafted-poly(acrylamide)/sodium alginate blend beads. Eur J Pharm Biopharm 65:204–214
27. Ali MHM, Kahder MM, Al-Saad KA, Al-Meer S (2013) Properties of nanoclay PVA composites materials. QSci connect 2013:1–9
28. Karimi A, Wan Daud WMA (2017) Materials, preparation, and characterization of PVA/MMT nanocomposite hydrogels: a review. Polym Compos 38:1086–1102
29. Zhou C, Tong D, Yu W (2019) Smectite nanomaterials: preparation, properties, and functional applications. In: Wang A, Wang W (eds) Nanomaterials from clay minerals. Elsevier, Amsterdam, pp 335–364
30. Ahmad R, Mirza A (2015) Sequestration of heavy metal ions by Methionine modified bentonite/Alginate (Meth-bent/Alg): a bionanocomposite. Groundw Sustain Dev 1:50–58
31. He YF, Zhang L, Yan DZ, Liu SL, Wang H, Li HR, Wang RM (2012) Poly(acrylic acid) modifying bentonite with in-situ polymerization for removing lead ions. Water Sci Technol 65:1383–1391
32. Rijith S, Anirudhan TS, Sumi VS, Anitha PK, Abhilash S, Shibli SMA (2015) Carboxylate functionalized Chitosan/Bentonite composite matrix as a cation exchanger for the removal of Pb(II) from aqueous media: Kinetic and equilibrium studies. Orient J Chem 31:1113–1120
33. Wang X, Yang L, Zhang J, Wang C, Li Q (2014) Preparation and characterization of chitosan–poly (vinyl alcohol)/bentonite nanocomposites for adsorption of Hg (II) ions. Chem Eng J 251:404–412
34. Baigorria E, Cano LA, Sanchez LM, Alvarez VA, Ollier RP (2020) Bentonite-composite polyvinyl alcohol/alginate hydrogel beads: Preparation, characterization and their use as arsenic removal devices. Environ Nanotechnol Monit Manag 14:100364
35. Sanchez LM, Alvarez VA, Ollier RP (2019) Acid-treated bentonite as filler in the development of novel composite PVA hydrogels. J Appl Polym Sci 136:47663
36. Rhoades J (1983) Cation exchange capacity. In: Page C (ed) Methods of soil analysis: Part 2 chemical and microbiological properties. ASA Press, Madison, pp 149–157
37. Öztürk N, Tabak A, Akgöl S, Denizli A (2008) Reversible immobilization of catalase by using a novel bentonite–cysteine (Bent–Cys) microcomposite affinity sorbents. Colloids Surf A 322:148–154
38. Fan L, Du Y, Wang X, Huang R, Zhang L, Hu L (2005) Preparation and characterization of alginate/poly (vinyl alcohol) blend fibers. J Macromol Sci A 42:41–50
39. Golafshan N, Rezahasani R, Tarkesh Esfahani M, Kharaziha M, Khorasani SN (2017) Nanohybrid hydrogels of laponite: PVA-alginate as a potential wound healing material. Carbohydr Polym 176:392–401

40. Hema M, Selvasekarapandian S, Arunkumar D, Sakunthala A, Nithya H (2009) FTIR, XRD and ac impedance spectroscopic study on PVA based polymer electrolyte doped with NH4X (X=Cl, Br, I). J Non-Cryst Solids 355:84–90
41. Jose T, George SC, Maria HJ, Wilson R, Thomas S (2014) Effect of bentonite clay on the mechanical, thermal, and pervaporation performance of the poly (vinyl alcohol) nanocomposite membranes. Ind Eng Chem Res 53:16820–16831
42. Hosseinzadeh H, Zoroufi S, Mahdavinia GR (2015) Study on adsorption of cationic dye on novel kappa-carrageenan/poly (vinyl alcohol)/montmorillonite nanocomposite hydrogels. Polym Bull 72:1339–1363
43. Morgan AB, Gilman JW (2003) Characterization of polymer-layered silicate (clay) nanocomposites by transmission electron microscopy and X-ray diffraction: a comparative study. J Appl Polym Sci 87:1329–1338
44. Ismail NHC, Akil HM (2018) Effects of organomodified muscovite on the properties of acrylonitrile–butadiene–styrene nanocomposites. J Appl Polym Sci 135:46827
45. Castellini E, Malferrari D, Bernini F, Brigatti MF, Castro GR, Medici L, Mucci A, Borsari M (2017) Baseline studies of the clay minerals society source clay montmorillonite stx-1b. Clays Clay Miner 65:220–233
46. Madejová J (2003) FTIR techniques in clay mineral studies. Vib Spectrosc 31:1–10
47. Slaný M, Jankovič Ľ, Madejová J (2019) Structural characterization of organo-montmorillonites prepared from a series of primary alkylamines salts: Mid-IR and near-IR study. Appl Clay Sci 176:11–20
48. Che C, Glotch TD, Bish DL, Michalski JR, Xu W (2011) Spectroscopic study of the dehydration and/or dehydroxylation of phyllosilicate and zeolite minerals. J Geophys Res Planets 116:1–23
49. Panhwar S, Hassan SS, Mahar RB, Canlier A, Sirajuddin AM (2018) Synthesis of l-cysteine capped silver nanoparticles in acidic media at room temperature and detailed characterization. J Inorg Organomet Polym Mater 28:863–870
50. Parsons JG, Dokken KM, McClure J, Gardea-Torresdey JL (2013) FTIR, XAS, and XRD study of cadmium complexes with l-cysteine. Polyhedron 56:237–242
51. Wu J, Yu H-Q (2007) Biosorption of 2, 4-dichlorophenol by immobilized white-rot fungus Phanerochaete chrysosporium from aqueous solutions. Bioresour Technol 98:253–259
52. Mansur HS, Sadahira CM, Souza AN, Mansur AA (2008) FTIR spectroscopy characterization of poly (vinyl alcohol) hydrogel with different hydrolysis degree and chemically crosslinked with glutaraldehyde. Mater Sci Eng C 28:539–548
53. Dong Y, Zhang L, Shen J, Song M, Chen H (2006) Preparation of poly (vinyl alcohol)-sodium alginate hollow-fiber composite membranes and pervaporation dehydration characterization of aqueous alcohol mixtures. Desalination 193:202–210
54. Mansur HS, Oréfice RL, Mansur AA (2004) Characterization of poly (vinyl alcohol)/poly (ethylene glycol) hydrogels and PVA-derived hybrids by small-angle X-ray scattering and FTIR spectroscopy. Polymer 45:7193–7202
55. Awadhia A, Agrawal S (2007) Structural, thermal and electrical characterizations of PVA: DMSO: NH4SCN gel electrolytes. Solid State Ion 178:951–958
56. Abd El-Latif M, El-Kady M, Ibrahim AM, Ossman M (2010) Alginate/polyvinyl alcohol-kaolin composite for removal of methylene blue from aqueous solution in a batch stirred tank reactor. J Am Sci 6:280–292
57. Shooto ND, Wankasi D, Sikhwivhilu LM, Dikio ED (2016) Modified electro-spun polyvinyl alcohol nanofibers used as super adsorbing material for lead ions in aqueous solution. J Residuals Sci Technol 13:233–242
58. Ren H, Gao Z, Wu D, Jiang J, Sun Y, Luo C (2016) Efficient Pb (II) removal using sodium alginate–carboxymethyl cellulose gel beads: Preparation, characterization, and adsorption mechanism. Carbohydr Polym 137:402–409
59. Pour ZS, Ghaemy M (2015) Removal of dyes and heavy metal ions from water by magnetic hydrogel beads based on poly (vinyl alcohol)/carboxymethyl starch-g-poly (vinyl imidazole). RSC Adv 5:64106–64118
60. Faghihian H, Nejati-Yazdinejad M (2009) Sorption performance of cysteine-modified bentonite in heavy metals uptake. J Serbian Chem Soc 74:189
61. USEPA (2009) Drinking water treatability database, GAC Isotherm, US Environmental Protection Agency, Cincinnati
62. Bulut Y, Aydın H (2006) A kinetics and thermodynamics study of methylene blue adsorption on wheat shells. Desalination 194:259–267
63. Yang H, Wang JH, Cheng KP, Yan MT, Qiao CZ (2013) Adsorption of Pb (II) on Hydroxyapatite/(Poly Vinyl Alcohol) Blend Material. Adv Mater Res 781:2253–2256
64. Hameed B, Mahmoud D, Ahmad A (2008) Equilibrium modeling and kinetic studies on the adsorption of basic dye by a low-cost adsorbent: Coconut (Cocos nucifera) bunch waste. J Hazard Mater 158:65–72
65. Igberase E, Osifo P, Ofomaja A (2018) Adsorption of metal ions by microwave assisted grafting of cross-linked chitosan beads: equilibrium, isotherm, thermodynamic and desorption studies. Appl Organomet Chem 32:4131
66. Jamnongkan T, Kantarot K, Niemtang K, Pansila PP, Wattanakornsiri A (2014) Kinetics and mechanism of adsorptive removal of copper from aqueous solution with poly (vinyl alcohol) hydrogel. Trans Nonfer Met Soc China 24:3386–3393
67. Abraham TN, Kumar R, Misra R, Jain S (2012) Poly (vinyl alcohol)-based MWCNT hydrogel for lead ion removal from contaminated water. J Appl Polym Sci 125:E670–E674
68. Teng H, Hsieh C-T (1999) Activation energy for oxygen chemisorption on carbon at low temperatures. Ind Eng Chem Res 38:292–297
69. Metwally SS, Rizk HE (2014) Preparation and characterization of nano-sized iron–titanium mixed oxide for removal of some lanthanides from aqueous solution. Sep Sci Technol 49:2426–2436
70. Sahmetlioglu E, Yilmaz E, Aktas E, Soylak M (2014) Polypyrrole/multi-walled carbon nanotube composite for the solid phase extraction of lead(II) in water samples. Talanta 119:447–451
71. Lim CW, Song K, Kim SH (2012) Synthesis of PPy/silica nanocomposites with cratered surfaces and their application in heavy metal extraction. J Ind Eng Chem 18:24–28
72. Nyairo WN, Eker YR, Kowenje C, Akin I, Bingol H, Tor A, Ongeri DM (2018) Efficient adsorption of lead (II) and copper (II) from aqueous phase using oxidized multiwalled carbon nanotubes/polypyrrole composite. Sep Sci Technol 53:1498–1510
73. Badruddoza AZM, Shawon ZBZ, Tay WJD, Hidajat K, Uddin MS (2013) Fe3O4/cyclodextrin polymer nanocomposites for selective heavy metals removal from industrial wastewater. Carbohydr Polym 91:322–332
74. Jiang N, Xu Y, Dai Y, Luo W, Dai L (2012) Polyaniline nanofibers assembled on alginate microsphere for Cu2+ and Pb2+ uptake. J Hazard Mater 215–216:17–24
75. Ghoul M, Bacquet M, Morcellet M (2003) Uptake of heavy metals from synthetic aqueous solutions using modified PEI—silica gels. Water Res 37:729–734
76. Nazarzadeh Zare E, Mansour Lakouraj M, Ramezani A (2016) Efficient sorption of Pb(ii) from an aqueous solution using a poly(aniline-co-3-aminobenzoic acid)-based magnetic core–shell nanocomposite. New J Chem 40:2521–2529
77. Ermolenko A, Vikulova M, Shevelev A, Mastalygina E, Ogbuna Offor P, Konyukhov Y, Razinov A, Gorokhovsky A, Burmistrov I

(2020) Sorbent based on polyvinyl butyral and potassium polytitanate for purifying wastewater from heavy metal ions. Processes 8:690

78. Khalek M, Mahmoud GA, El-Kelesh NA (2012) Synthesis and characterization of poly-methacrylic acid grafted chitosan-bentonite composite and its application for heavy metals recovery. Chem Mater Res 2:16